A Semi-Transmissive Cylindrical Metasurface Enabled Dual-Band Shared-Aperture DRA

Xing-Yu Cheng
Global Big Data Technologies Centre
University of Technology Sydney
Sydney, Australia
xingyu.cheng@student.uts.edu.au

Can Ding
Global Big Data Technologies Centre
University of Technology Sydney
Sydney, Australia
can.ding@uts.edu.au

Richard W. Ziolkowski
Department of Electrical and Computer Engineering
University of Arizona, Tucson AZ USA
ziolkows@arizona.edu

***Abstract*— Minimizing antenna size continues to pose significant challenges in various applications. This paper presents the integration of two cylindrical dielectric resonator antennas (DRAs) into a compact shared-aperture configuration. We introduce two structures designed to reduce scattering and coupling, ensuring the independent operation of the DRAs despite their shared aperture. To validate our approach and optimized design, its prototype was subjected to both extensive simulations and experimental measurements.**

Keywords—Compact, cross-band scattering and coupling, dielectric resonator antenna (DRA), metasurface, shared-aperture

I. Introduction

Given cost and space constraints, modern communication systems often require the integration of multiple antennas on a single platform [1-2]. However, such compact arrangements can lead to substantial cross-band interference, jeopardizing radiation patterns and port isolation [3]. Dielectric resonator antennas (DRAs) have been extensively studied for years and have garnered considerable interest due to their wide bandwidth and ease of excitation [4]. This paper introduces a compact shared-aperture design that seamlessly integrates two cylindrical DRAs by equipping it with a descattering structure comprised of a conformal metasurface and modified slot lines. The operating modes within these DRAs are also explored. Simulated and measured results validate the efficacy of the design approach, demonstrating its exceptional potential for multifunctional antenna systems.

II. Design and Mechanisms of DRAs

A. Antenna configuration

Fig. 1 illustrates the design of the prototyped dual-band shared-aperture DRA. As shown in Fig. 1(a), two cylindrical DRAs are concentrically mounted on a substrate which facilitates their feed lines. The low band (LB) DRA (green) is activated by an side-fed metallic post via a microstrip line from port 1, while the high band (HB) DRA (orange) uses a modified slotline and is fed from port 2. A conformal metasurface is positioned in the air gap between the DRAs.

This dual-band shared-aperture DRA was developed from two independent DRA elements. Initially, without any descattering or decoupling structures, the port isolation in the LB was merely 5.9 dB. Moreover, the radiation pattern in the HB was negatively impacted. To enhance the port isolation, the original straight slot was replaced by a modified slot. As shown in Fig. 1, the modified slot consists of two mirror-symmetric C-shaped slots. Each slot corresponds to a half-wavelength in the LB, and one and a half wavelengths in the HB. This configuration ensures opposite fields in the LB and reinforced fields in the HB. Consequently, the port isolation $|S_{12}|$ has improved from 5.9 dB to above 25 dB from 3.4-4.0 GHz without compromising transmission in the HB. This outcome is shown in Fig. 2(a).

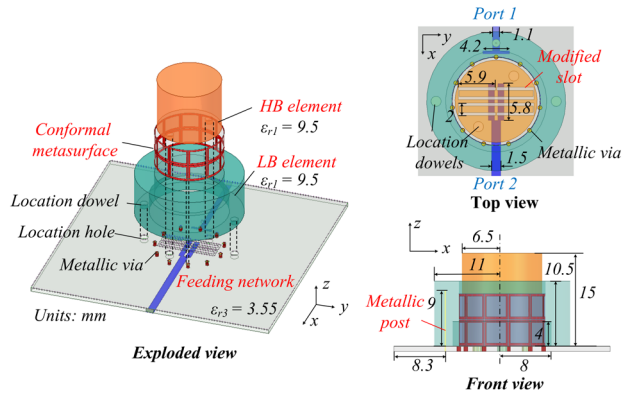

Fig. 1. Experimentally-verified dual-band shared-aperture DRA design.

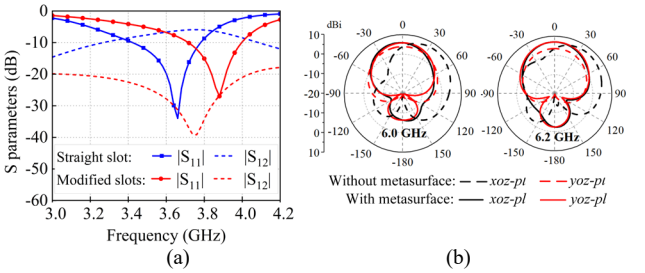

(a) (b)

Fig. 2. (a) Simulated S-parameters when incorporating the straight and modified slots. (b) Comparison of the simulated HB radiated field with and without the innovative, custom-designed conformal metasurface.

The conformal metasurface array developed to recover the independent operation of the DRAs is shown in Fig. 1. It consists of twenty-two units configured in an 11 × 2 grid. Each unit cell of the metasurface is comprised of a rectangular ring strip, measuring 3.8 mm × 4.1 mm. Simulations in HFSS confirmed that it exhibits a reflection response from 5.3 to 8.2 GHz and a transmission response from 3.7 to 4.9 GHz. It is constructed on a flexible substrate that forms a complete ring when it is introduced between the two DRAs. The total height of metasurface is lower than that of the HB DRA. Its semi-transmissive characteristics are critical to the restoration of the radiated field performance of each DRA.

Fig. 2(b) displays the simulated HB realized gain patterns with and without the presence of the conformal metasurface. It is evident that significant improvements are obtained when the metasurface is present. The distortions in the *xoz*-plane have markedly diminished and a gain increase to 6.5 dBi in the *yoz*-plane was achieved. These results demonstrate the effectiveness of the custom-designed metasurface in restoring and even boosting the HB radiation performance.

B. Analysis on operating modes

The operating modes of the inner DRA evolved during the design process. The operating mode of the outer DRA consistently remained in the $HEM_{11\delta}$ ($0<\delta<1$) mode. The electric field vector distribution in Fig. 3 (a) demonstrates that

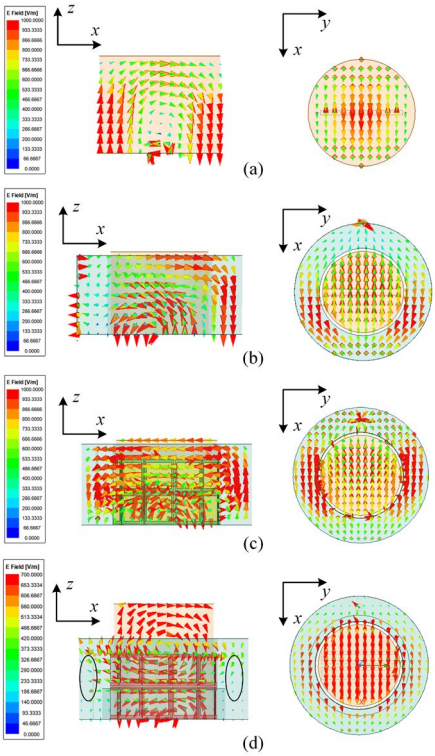

Fig. 3. Electric field distribution of HB elements at 6.2GHz. (a) Single HB DRA. HB DRA in an interim shared-aperture configuration (b) without, (c) with metasurface presented. (d) HB DRA in final shared-aperture configuration with metasurface presented.

when the single HB DRA is exclusively excited, it operates in the $HEM_{11\delta}$ mode at its center frequency, 6.2 GHz. The electric field distribution in an interim configuration with and without the presence of the metasurface is compared in Figs. 3(b) and (c). The LB and HB elements retained their initial heights (LB DRA: 10.5 mm, HB DRA: 11 mm) in this case. It is found that the introduction of the metasurface yields an undistorted field distribution in the *xoy*-plane that is now uniform along the *x*-axis. However, the reflection coefficients within the HB in this interim configuration with the metasurface measure around 6 dB, suggesting that the DRA is not significantly resonating. Therefore, the operating mode is not defined in this condition. In the final configuration in Fig. 3 (d), the height of the HB DRA was increased from 11 mm to 15 mm to compensate for the input impedance change caused by the metasurface. This adjustment ensured that the integrated DRAs resonated at their LB and HB frequencies. With the increased height the HB mode shifted operating in the $HEM_{11\delta+2}$ mode. Furthermore, as highlighted by the black circles, the electric field at the bottom is constrained while the top part leaks out. This demonstrates additional semi-transmissive properties of the custom-designed metasurface.

C. Experimental validation

The component of the optimized dual-band shared aperture DRAs were fabricated, assembled, and tested as shown in Fig. 4. The simulated and experimental S-parameters are compared in Fig. 5. Fig. 5 (a) indicates that the experimental LB and HB bandwidths ($|S_{11}|$< -10 dB|) are 14% (3.5 to 4.0 GHz) and 12% (5.8 to 6.5 GHz), respectively. The cross-band coupling has decreased by more than 20 dB in both bands. The simulated and measured radiation patterns

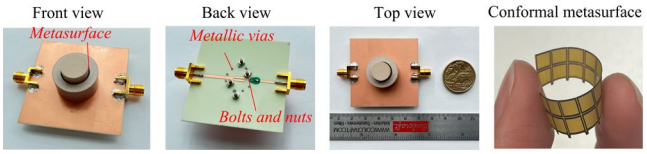

Fig. 4. Prototype of presented dual-band cylindrical DRA and conformal metasurface.

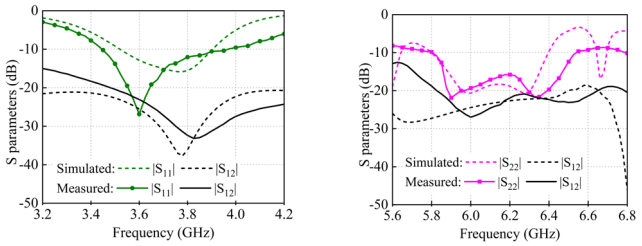

Fig. 5. Comparisons of simulated and measured S-parameter of presented dual-band cylindrical DRA.

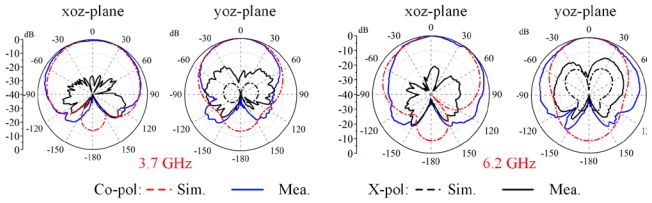

Fig. 6. Comparisons of simulated and measured radiation patterns at LB center frequency and HB center frequency respectively.

are presented in Fig. 6. It is clear that the LB DRA's radiated field performance remained the same (very good) and that of the HB DRA's original performance was recovered from the scattering and coupling-induced distortion. Therefore, the cross-band interference issues in this compact DRA were solved by introducing the custom-designed metastructure.

III. Conclusion

In this study, two cylindrical DRAs were collocated to achieve miniaturization. The challenges of decreased port isolation and skewed radiation patterns due to cross-band interference were addressed with a modified slot excitation of the HB DRA and the introduction of a custom-designed conformal metasurface. Experimental tests were conducted and verified its simulated performance characteristics. The measured results indicate that the port isolation was improved from 6 dB to over 25 dB within the low band. Furthermore, the radiation patterns of the HB element were substantially corrected. The study of the DRA modes confirmed that the integrated dual-band cylindrical DRA operates in the $HEM_{11\delta}$ and $HEM_{11\delta+2}$ modes in the LB and HB, respectively.

References

[1] S.-Y. Sun, C. Ding, W. Jiang, and Y. J. Guo, "Simultaneous suppression of cross-band scattering and coupling between closely spaced dual-band dualpolarized antennas," *IEEE Trans. Antennas and Propag.*, vol. 71, no. 8, 2023.

[2] H. -H. Sun, C. Ding, H. Zhu, B. Jones and Y. J. Guo, "Suppression of cross-band scattering in multiband antenna arrays," *IEEE Trans. Antennas and Propag.*, vol. 67, no. 4, pp. 2379-2389, Apr. 2019.

[3] Y. J. Guo and R. W. Ziolkowski, Advanced antenna array engineering for 6G and beyond wireless communications. 1st ed. Hoboken, NJ, USA: Wiley, 2021.

[4] Y. M. Pan, X. Qin, Y. X. Sun, and S. Y. Zheng, "A simple decouplingmethod for 5G millimeter-wave MIMO dielectric resonator antennas," *IEEE Trans. Antennas and Propag.*, vol. 67, no. 4, pp. 2224–2234, 2019.